ACS OMEGA

Open Access

http://pubs.acs.org/journal/acsodf

Article

Tandem MS Elucidation of the Late-Stage Degradation Mechanism of Nitroplasticizer

Kitmin Chen* and Dali Yang*

Cite This: *ACS Omega* 2024, 9, 36600−36608

Read Online

ACCESS | Metrics & More | Article Recommendations | Supporting Information

ABSTRACT: Understanding the degradation behavior of nitroplasticizer (NP) and the subsequent production of nitro-organics is crucial for both environmental monitoring and material development. A nontargeted approach via LC-QTOF-MS was employed to thoroughly study the degradation mechanism of NP in its late aging stage. Both positive and negative modes of ESI were performed to increase the compound coverage. To shed light on the fragmentation behavior of NP degradants (e.g., compounds containing a high density of NO_2 moieties and oxygen sites) in the positive mode, which is rarely reported, the high-resolution tandem MS information on precursor ions at m/z 251(+), 254(+), 266(+), and 270(+) and a pair of isomeric ions at m/z 284(+) was investigated to extract their common diagnostic ions and dissociation channels, including the neutral loss of 2,2-dinitropropanol, nitro-nitrite rearrangement, homolytic cleavage of NO_2, and simple inductive cleavage. Additionally, leveraging the sensitivity for nitroaromatics in the negative polarity, negative ions m/z 182(−) and 233(−) are identified as dinitroaniline and dinitronaphthol, respectively, which confirm the secondary hydrolysis pathway of the antioxidant (e.g., *N*-phenyl-2-naphthylamine) postulated in our previous work. In addition to earlier findings, the detection of these eight degradants further supports the evidence of increased acid concentration and aging temperatures in the late-stage NP environment, which contribute to intricate degradation behaviors in different aging environments.

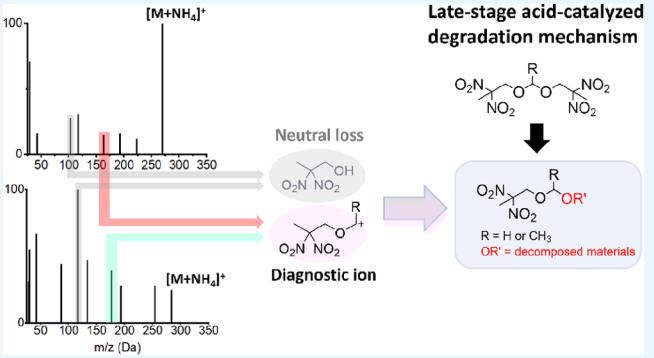

1. INTRODUCTION

Nitro-organics are prevalent environmental pollutants found in industrial processes, energetic materials, biomass burning, and combustion emissions.[1−4] Therefore, understanding the mechanism of their formation and degradation is essential for effective environmental monitoring. Recent oxidative studies conducted by Guzman, Rana, and others have revealed numerous reaction pathways between radicals (e.g., HO or NO_x) or strong electrophiles (e.g., NO_2^+) and phenolic compounds (e.g., catechols) in the air−water and air−solid interfaces, resulting in the formation of hydroxylated, nitrated, and oligomerized species.[1−3,5,6] In the aging process of nitroplasticizer (NP), a binder component commonly used in propellant and explosive composites to reduce mechanical sensitivity and improve processability of explosive materials,[7−9] similar reactive species such as HNO_x, NO_x, H_2O, etc., can be generated[10−12] though there is a systematic difference between atmospheric aerosols and energetic materials. Consequently, these reactive species can consumethe antioxidant, *N*-phenyl-2-naphthylamine (PBNA), leading to advanced NP degradation and triggering cascade production of various nitro-organics during NP aging at different stages.

The NP studied here is the eutectic mixture of 1:1 bis(2,2-dinitropropyl) acetal/formal (BDNPA/F) that contains ∼0.1 wt % PBNA as the stabilizer.[13] Between 2000 and 2008, a 156 week-long constituent aging study of 1100 NP-containing samples was conducted,[10,11] profiling various gaseous products and demonstrating the degradation of NP even under mild conditions (40−64 °C). However, the changes in the compositions of NP alone were not systematically evaluated, which make it difficult to understand the degradation mechanism and kinetics. In the following 24 month-long aging experiment at 70 °C, the molecular changes in NP were detected by the formation of new functional groups, such as hydroxyl (−OH), ketone (>C═O), and alkene (>C═C<).[14] Based on these considerations, a comprehensive study on NP aging behaviors was conducted over a longer duration (44 months) and at mild temperatures (≤64 °C) in 2016.[15−17] In the following years, the roles of headspace,[16] water,[18] PBNA,[19] and acids[20] have been studied[21] using various chemical characterization techniques (e.g., FTIR, NMR, and UV/vis) to understand the impacts of NP

Received: May 24, 2024
Revised: July 20, 2024
Accepted: August 6, 2024
Published: August 15, 2024

Table 1. LC Parameters

	ESI− mode	ESI+ mode
mobile phases	A: 13 mM ammonium acetate in water, pH 6.0	A: 0.1% formic acid in water
	B: 13 mM ammonium acetate in 95:5 (v/v) ACN, pH 6.0	B: 0.1% formic acid in methanol
needle rinse	0.02% formic acid and 5% acetone in ACN	0.02% formic acid and 5% acetone in ACN
run time (min)	18	16
gradient program (% B)	0.00 min (20.0%), 3.00 min (60.0%), 10.0 min (60.0%), 10.1 min (99.9%), 14.0 min (99.9%), 14.1 min (20.0%)	0.00 min (60.0%, curve at −1), 10.0 min (99.9%), 10.1 min (99.9%), 12.6 min (99.9%), 12.7 min (60.0%)
flow rate (mL/min)	acquisition and equilibration = 0.35	acquisition and equilibration = 0.30
	[a]column rinse = 0.50	[a]column rinse = 0.50
[b]valve method (min)	1.2−9.0	1.0−9.0

[a]Column rinse is applied after the 9 min mark and continues until the end of each injection. [b]Valve method specifies the time range for data acquisition by switching the divert valve to direct eluents from column to MS.

degradation on the energetic material applications and facilitate any necessary remediations.

The use of liquid chromatography tandem quadrupole time-of-flight mass spectrometry (LC-QTOF-MS) and ion chromatography (IC) has played a significant role in revealing details at different stages of NP degradation mechanisms, including the identification of nitroso-PBNA[22] as an abundant early-stage degradant of PBNA that also served as an effective antioxidant in scavenging NO_x generated from HONO decomposition,[8,10,11,14,17] dinitro-PBNA as a pivotal degradant that determines the initiation of NP degradation, and acetic/formic acids as part of the terminal products alongside with 2,2-dinitropropanol (DNPOH).[23,24] However, there are still a great number of late-stage species uncovered in the nontargeted survey of long-term aged NP samples, particularly in the MS scans of positive polarity, which detected twice the number of potential species than those of negative polarity.[25] Typically, negative polarity in MS is used to analyze aliphatic nitro compounds for enhanced sensitivity, which is related to the negative polarization induced by the NO_2 groups; the hydrogen atoms of the hydrocarbon groups within the molecule (e.g., methylene, $-CH_2-$) become positively polarized and thus facile for exoergic deprotonation or adduct formation with anions.[26,27] Therefore, the literature on tandem MS analysis of the aliphatic nitro compounds with positive polarity is often limited.

In a nontargeted approach to material aging studies, the elucidation of the degradation mechanism relies greatly on the extent of information available. Leveraging the use of both positive and negative polarities in electrospray ionization (ESI) and the structural information obtained from collisional-induced dissociation (CID), a total of eight more new compounds associated with the late-stage degradation of NP and PBNA are elucidated in the present paper, in addition to the numerous compounds identified in earlier studies.[10,19−23,25] The fragmentation behavior of NP-related degradants in the positive polarity is discussed, including their possible origins given by the tandem MS information.

2. EXPERIMENTAL SECTION

The baseline NP samples prepared in PTFE-capped glass vials were either sealed in air (denoted as air-aged) or added deionized water on top of NP (denoted as water-aged) for capturing volatile species and were then subjected to thermal aging from 0 to 44 months at four temperatures (38, 45, 55, and 64 °C)[15−17] (see the Supporting Information, Aging Sample Preparation). Solutions of aged NP were prepared by dissolving 3.0 ± 0.5 mg in 10 mL of acetonitrile (ACN). The analysis was performed using a SCIEX ExionLC system coupled with a X500R QTOF-MS instrument operated at information-dependent acquisition (IDA) mode. Chromatography was achieved with a Kinetex C8 reverse phase column (2.6 μm, 150 × 3.0 mm) held at 40 °C. The parameters are provided in Tables 1 and 2. Automated mass calibration within a 5 ppm tolerance was conducted every two sample injections using ESI (±) SCIEX POS calibration solutions. In positive mode, calibrated masses ranging from m/z 132 to 609 were used for TOF MS, and those ranging from m/z 174 to 448 of the parent ion m/z 609 were used for TOF MS/MS. In negative mode, calibrated masses ranging from m/z 113 to 521 were used for TOF MS, and those ranging from m/z 113 to 521 of the parent ion m/z 793 were used for TOF MS/MS. A mass accuracy of 10 ppm is adopted for the determination of elemental compositions, which is typical for mass spectrometers with a minimum resolution of 10,000.[28] In all figures of MS/MS spectra, the tentative assignments are labeled with the corresponding observed mass and mass accuracy. The percentage relative abundances (RAs) presented in the figures were calculated by dividing the maximal intensity (I_{max}) and used only for qualitative assessment (not quantitative). Note that the RAs do not reflect their concentrations in the samples.

Table 2. MS^1/MS^2 Parameters (Sciex X500R)

source parameters		
source gas 1 and 2 (psi)	50	50
curtain gas (psi)	30	30
source temperature (°C)	300	250
spray voltage (V)	−4500	5500
CAD gas (psi)	9	9
scan cycle	1759	2814
total scan time (s)	0.341	0.341
IDA parameters	**MS^1/MS^2(−)**	**MS^1/MS^2(+)**
range (m/z)	80−650/25−580	75−650/25−500
declustering potential (V)	−80 ± 5/−50 ± 5	80 ± 5/70 ± 5
collision energy, CE (V)	−10/−27 ± 15	10/25 ± 15
accumulation time (s)	0.1/0.05	0.1/0.05
candidate precursor ions per cycle	4	4
IDA intensity threshold (cps)	500	500

3. RESULTS AND DISCUSSION

3.1. Positive Polarity. *3.1.1. Positive Ionization.* The negative polarization induced by NO_2 groups in nitro compounds (e.g., nitroalkanes) has a determinative impact on

https://doi.org/10.1021/acsomega.4c04923
ACS Omega 2024, 9, 36600−36608

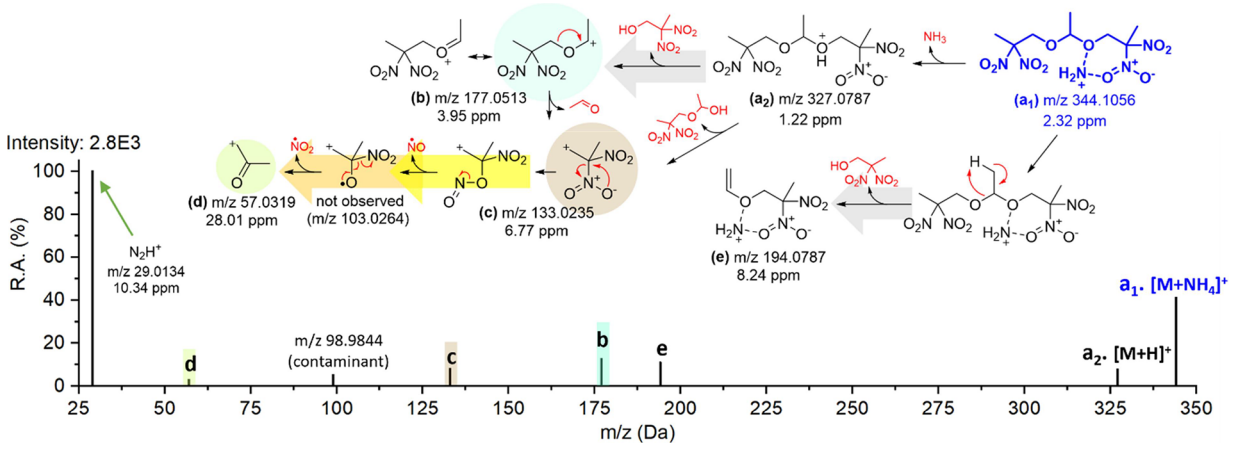

Figure 1. Representative fragment ion spectrum of m/z 344 (BDNPA, $[C_8H_{12}N_4O_{10}+NH_4]^+$, retention time ($T_R$) at 4.08 min). Proton transfer coupling with loss of NH_3: $\mathbf{a_1}$ (m/z 344) → $\mathbf{a_2}$ (m/z 327). Inductive cleavages: **b** → **c** (m/z 133, a common ion between BDNPA and BDNPF, brown circle) and the neutral loss of DNPOH (gray arrow) from $\mathbf{a_1}$ → **e** (m/z 194) and $\mathbf{a_2}$ → **b** (m/z 177, a BDNPA-associated ion, light blue circle). Nitro-nitrite rearrangement (yellow arrow) coupling with the homolytic losses of NO and consequently NO_2 (orange arrow): **c** → **d** (m/z 57, light green circle); predicted intermediate m/z 103.0264 is not observed. m/z 29 (N_2H^+) and m/z 98.9844 are proposed as background ions of unknown origin.

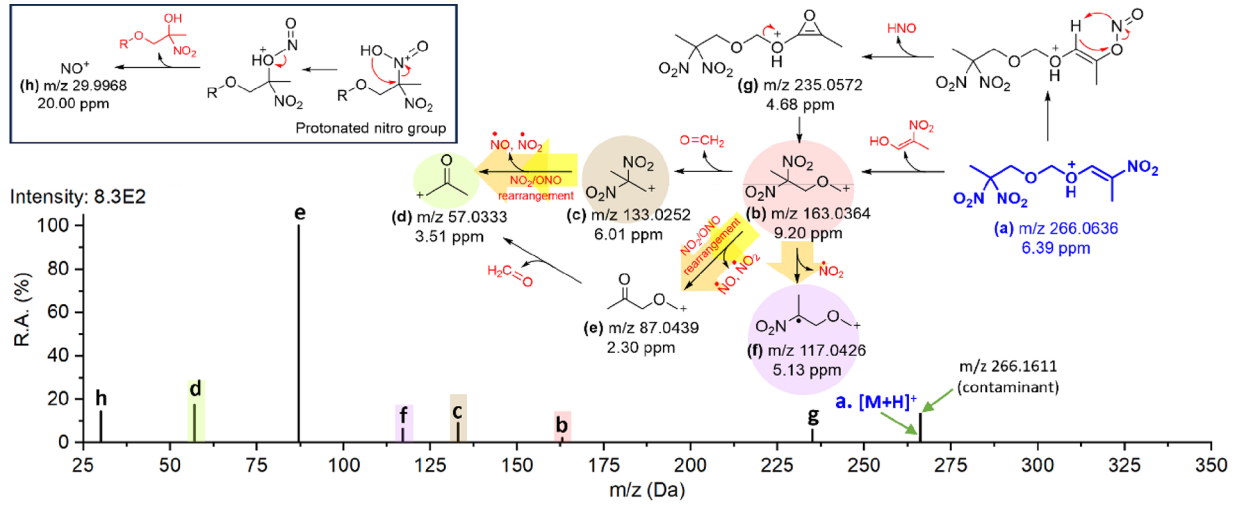

Figure 2. Representative fragment ion spectrum of m/z 266 ($[C_7H_{11}N_3O_8+H]^+$, T_R at 3.00 min). Inductive cleavages: **a** → **b** (m/z 163, a BDNPF-associated ion, pink circle) and → **c** (m/z 133, a common ion between BDNPA and BDNPF, brown circle). Nitro-nitrite rearrangement with NO (yellow arrow) and NO_2 radical losses (orange arrow): **c** → **d** (m/z 57, light green circle) and **b** → **e** (m/z 87). Competitive homolytic cleavage of NO_2 (also orange arrow): **b** → **f** (m/z 117, a confirmatory ion unique to m/z 163, light purple). Rearrangement reactions led to the HNO loss from **a** → **g** (m/z 235) or formation of NO^+ ion (**h**) (m/z 30).

their ionization and fragmentation behavior. Protonation is often not the most prominent reaction for this class of compounds because the two oxygen atoms can bridge with an ammonium or metal ion to form a stable adduct ion through electrostatic interaction.[29] However, fewer CID fragment ions are often exhibited when stabilized by a metal ion (e.g., the sodiated ion of 2,3-dimethyl-2,3-dinitrobutane, [DMNB +Na]$^+$),[30] which reduce the structural information available for unknown identification. Therefore, the sodiated ions found in the aged NP samples have been omitted from this analysis. Unlike the sodiated ions, proton transfer can occur in ammonium adduct ions, as shown in Figure 1($\mathbf{a_2}$), allowing the propagation of fragmentation. The ammonium adduct ions are the dominant species found in the samples due to the use of ammonium acetate as an additive in the mobile phase. There are many oxygen sites for adduct formation and protonation in the NP degradants, a mechanism likely involving the stabilization via a six-membered ring configuration between the NO_2 group and the nearby oxygen site or between oxygen sites.

3.1.2. Dissociation Reactions. In a low-energy CID, the wide distribution of internal energy enables many dissociation channels and multiple generations of product ions. To better understand the fragmentation reactions in NP-related degradants and to identify their potential commonalities and signature fragment ions, the ammonium adduct ion of BDNPA is examined as a reference, as demonstrated in Figure 1. The candidate ion structures are logically deduced based on mass accuracy, the traceability of their molecular formula to the precursor ion, and the feasibility of dissociation pathways. Because of the highly polarized nature of BDNPA, simple inductive cleavage is favored, such as the weakening of the C−O bonds to facilitate $\mathbf{a_2}$ → **b** and **b** → **c**. The generation of m/z 194 (**e**) corresponds to the neutral loss of DNPOH (gray arrow). Although the described mechanism ($\mathbf{a_1}$ → **e**) may not seem favorable due to the required internal energy (E > 8 eV,

https://doi.org/10.1021/acsomega.4c04923
ACS Omega 2024, 9, 36600−36608

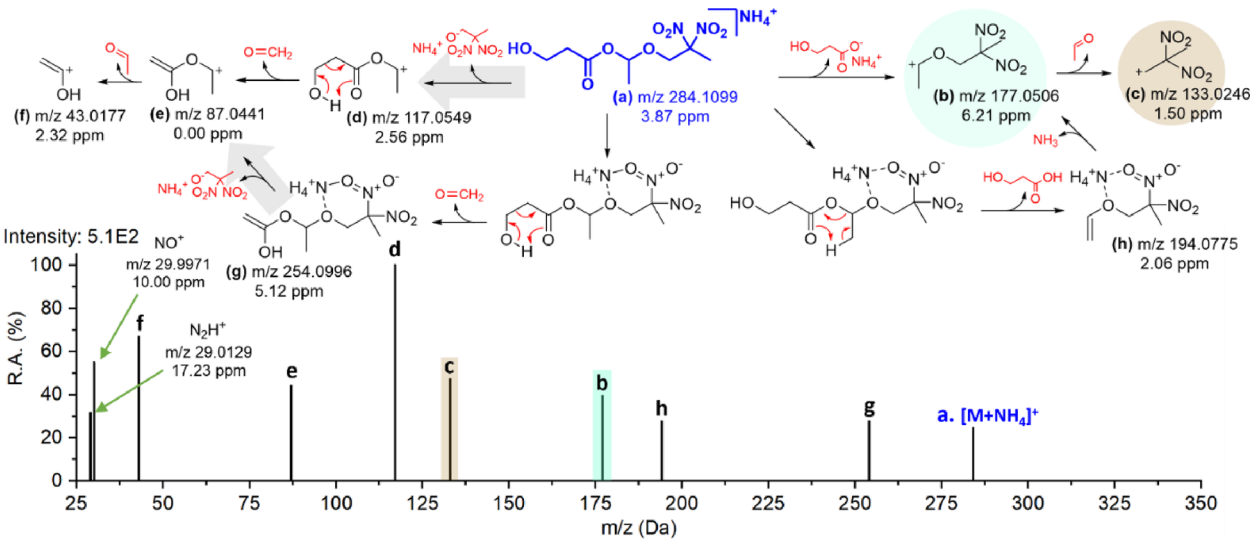

Figure 3. Representative fragment ion spectrum of m/z 284b ($[C_8H_{14}N_2O_8+NH_4]^+$ isomer, T_R at 2.73 min). Inductive cleavages: **a** → **b** (m/z 177, a BDNPA-associated ion, light blue circle) → **c** (m/z 133, a common ion between BDNPA and BDNPF, brown circle); neutral losses of DNPOH (gray arrows) from **a** → **d** (m/z 117) and **g** → **e** (m/z 87), and **d** → **e** (m/z 87) → **f** (m/z 43). Retro-aldol reactions: **a** → **g**, **a** → **h** (m/z 194), and **d** → **e**. Proton transfer with NH_3 loss: **h** → **b**. The m/z 117.05 presented here is different from the homolytic product ion m/z 117.04 in Figures 2 and 4 by >80 ppm in mass.

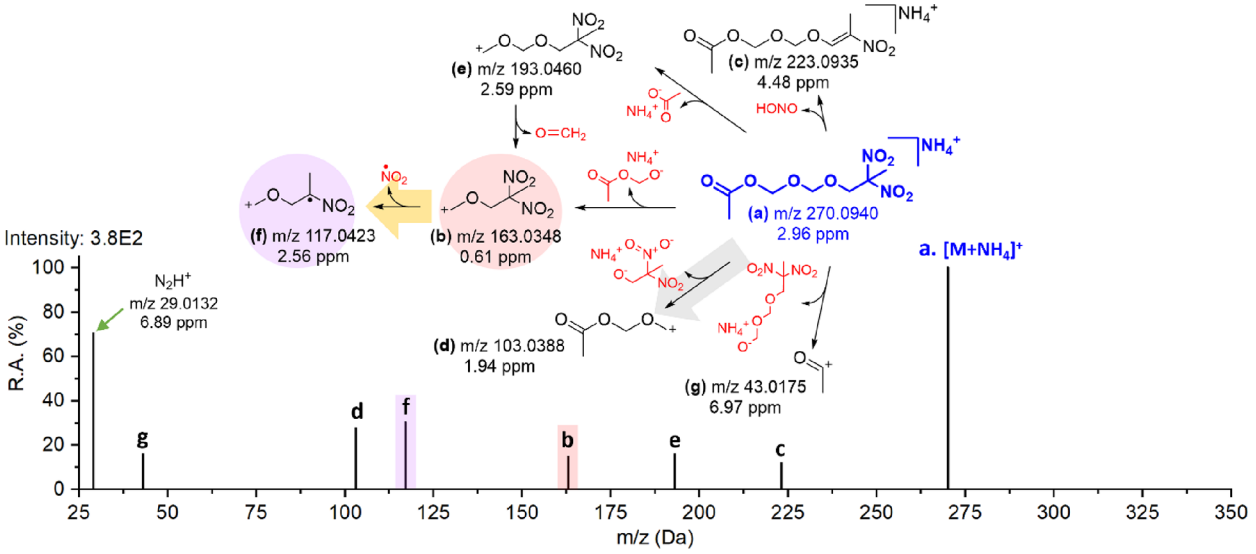

Figure 4. Representative fragment ion spectrum of m/z 270 ($[C_7H_{12}N_2O_8+NH_4]^+$, T_R at 2.30 min). Inductive cleavages: **a** → **b** (m/z 163, a BDNPF-associated ion, pink circle); neutral loss of DNPOH (gray arrow) from **a** → **d** (m/z 103); **a** → **e** (m/z 193) → **b**; and **a** → **g** (m/z 43). Homolytic cleavage of NO_2 (orange arrow): **b** → **f** (m/z 117, a confirmatory ion unique to m/z 163, light purple). Intramolecular HONO elimination: **a** → **c**.

estimated using average bond energies) for remote cleavage of both C−H and C−O bonds, the cumulative effect of multiple collisions with N_2 gas at the laboratory collision energy of 25 eV (E_{cm} = 2 eV, estimated energy transferred upon each collision in the center-of-mass frame, see the Supporting Information, E_{cm} Calculation) can lead to such a complex fragmentation outcome. Therefore, the fragment ion structure resulting from $\mathbf{a_1}$ → **e** is feasible particularly when ion stability through adduct coordination remains intact. Also, alternative candidates cannot be determined as other molecular formulas are either unable to trace back to the precursor ion or outside of the acceptable mass accuracy (e.g., 10 ppm).

The even-electron rule does not apply to the structural elucidation of nitro-compounds, as exemplified by the common dissociative losses of NO and NO_2 radicals.[31,32] The dissociation channel of **c** → **d** in Figure 1 suggests a NO loss with nitro-nitrite intramolecular rearrangement (yellow arrow: C-NO_2 → C-ONO), resulting in the homolysis of NO_2 (orange arrow). Nitro-nitrite isomerization is a competitive reaction to the direct C-NO_2 dissociation and involves a lower energy barrier in comparison.[33,34] Also, the tendency toward isomerization increases as the molecular stability decreases with the increasing number of NO_2 groups on the same carbon atom.[34] Because of an elongated C−O bond and a shortened O−N bond in the nitrite isomer, homolytic cleavage of NO is facile, which further induces the expulsion of NO_2 and decomposes to a relatively more stable carbonyl fragment ion (**d**) in the latter process. Hence, m/z 57 (**d**) is detected, whereas m/z 103 is not. The poor mass accuracy of m/z 57 (**d**) can be attributed to the fluctuation in kinetic energies caused by ionization or

https://doi.org/10.1021/acsomega.4c04923
ACS Omega 2024, 9, 36600−36608

fragmentation, inhomogeneous electric fields, or different ion mobility. If the ion falls outside the calibrated mass range, the optimized settings for applying the potential to accelerate ions into the flight tube may become inaccurate, resulting in variations in ion flight time and subsequently in m/z measurement. Some background or contaminant ions are also expected because the aged NP samples are complex mixtures of many unknown compounds, such as m/z 98 (e.g., the closest formula is $C_3HNO_3^+$ with a mass accuracy of 108.03 ppm) and m/z 29 (e.g., N_2H^+, typically formed by the reaction between H_2 and N_2).[35,36]

The MS/MS spectra of m/z 266, 284b, and 270 are presented in Figures 2, 3, and 4, respectively (m/z 251, 254, and 284a in Figures S1, S2, and S3 , respectively). Dissociation channels found in BDNPA such as nitro-nitrite rearrangement and/or homolytic cleavage of NO_2 are shared among m/z 251, 266, 270, and 284b. The most prominent characteristics are derived from simple inductive cleavage, which include the neutral loss of DNPOH. The fragment ion spectra of m/z 266, 284b, and 270 are utilized as representative examples because they contain the most fragment ions and are the least straightforward to elucidate. The characteristic dissociation channels and fragment ions are color-coded. As described in Scheme 1, when the protonation or

Scheme 1. Proposed Inductive Dissociation Pathways of NP Degradants in MS/MS[a]

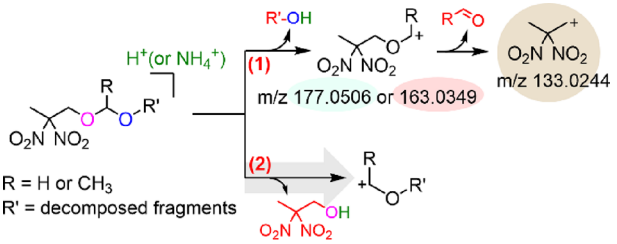

[a](1) Generation of characteristic fragment ions m/z 177.0506 or 163.0349 and subsequently 133.0244 and (2) the neutral loss of DNPOH.

adduct formation is localized in the acetal or formal region (e.g., O−CR−O), either R'−OH or DNPOH (or DNPOH$^-$ NH_4^+) can be inductively dissociated as neutral molecules. Reaction 1 is demonstrated by channels **a** → **b** → **c** in Figures 2 and 3. The formations of fragment ions m/z 177 or 163 (light blue or pink, respectively) and the shared subsequent fragment ion m/z 133 (brown) suggest that the origin of the degradant corresponds to either BDNPA or BDNPF, respectively. The fragment ion m/z 163 is also observed in m/z 270 (Figure 4 (**b**)). Although m/z 133 is not found, the homolytic loss of NO_2 from **b** → **f** in Figure 4 implies the same ion, m/z 117, and is also observed in channel **b** → **f** of m/z 266 in Figure 2 (as well as m/z 251 in Figure S1). On the other hand, Reaction 2 is an inductive cleavage assisted by the neutral loss of DNPOH, which is demonstrated by channels **a** → **d** in Figures 3 and 4 (also m/z 284a in Figure S3). In degradants containing multiple oxygen sites, competition between sites for protonation or adduct formation may change the distribution of the fragment ions. As a result, other product ions of inductive cleavages can be generated, and they are tentatively assigned to elucidate the remaining structure, such as channels **a** → **e** and **a** → **g** in Figure 4. Strictly in m/z 254 and 284a (Figures S2 and S3), although m/z 177 or 163 is not directly detected, the structures are likely explained by the inductive cleavage mechanism.

Beside the above-mentioned fragmentation mechanisms, other types of unimolecular reactions can also occur, such as the rare occasion of HNO loss[31] in channel **a** → **g** of Figure 2, the formation of NO^+ ion subsequent to the rearrangement of protonated nitro group[37] in Figure 2 (**h**), and the retro-aldol fragmentation[38] in channels **a** → **g**, **a** → **h**, and **d** → **e** of Figure 3. Although some of the m/z shares the same value, such as m/z 87 (**e**) in Figures 2 and 3, they are unrelated due to differences in dissociation origin, ion structure, and the product ion in the subsequent step. It is worth noting that the proposed structures cannot be conclusively confirmed due to the lack of commercial reference standards and the limited quantity of aged NP samples to perform fractionation.

3.1.3. Evolution of Late-Stage Degradants. Time evolution of degradants in NP samples aged at 55 and 64 °C is presented in Figure 5, and their absence at low temperatures (e.g., 38 and 45 °C) indicates that these products were generated at the late-stage of NP aging when it is aged at the elevated temperatures. Based on the PBNA nitration mechanism identified in our previous study,[19] the late-stage of NP degradation can be precisely marked by the depletion of dinitro-PBNA after 28 and 16 months of aging in the air-aged NP samples at 55 and 64 °C, respectively. Concurrently, these six NP degradants in the air-aged samples share similar timestamps. In both the air- and water-aged samples, their accelerated growth exhibits great resemblance to the previously observed sharp increase in acetic/formic acids and DNPOH from NP hydrolysis,[20] indicating that their formation is also promoted by the increased concentration of acidic species trapped in the sample matrix. Therefore, the mechanism is analogous to the acid-catalyzed mechanism of NP as proposed in Scheme 2; the oxonium ion can be attacked by the nucleophilic degraded fragments (e.g., HO-R') to form the NP degradants.[23,24,39−41] The degraded fragments are derived from either higher orders of decomposed products of NP or impurities proposed by Rindone et al.[42] The latter is unlikely because the quantity of impurities is less than 2% in the NP samples.[43] Therefore, if the reaction products are truly derived from impurities, then these impurities are not responsible for NP degradation because they do not participate in any meaningful reactions until the later stage, similar to our reported finding of DNPOH.[19,20] Based on the relationship described in Scheme 1, only m/z 284b is associated with BDNPA, whereas other species are associated with BDNPF, which implies that the hydrolytic kinetics in BDNPA is more rapid than BDNPF and likely leads to a higher order of decomposition (e.g., DNPOH, acetic acids, and other potential smaller fragments) instead of reacting with degraded fragments at the oxonium stage. Our simulation results also show a greater susceptibility of hydrolysis in BDNPA over BDNPF under acidic conditions.[21] Two noticeable observations in the NP degradants between the air- and water-aged samples indicate a more prominent formation of nitro-organics in the former ones and demonstrate their different degradation behaviors when environmental conditions are altered: (1) higher abundance and more degradation species are associated with the dry aging process, such as m/z 270 and 284b, and (2) the formation rates of m/z 251, 254, 266, and 284a do not significantly increase when aging with an aqueous layer above the matrix at 55 °C and below. It is suspected that some water soluble molecules, e.g., acidic molecules, were removed from the NP phase, which reduce their reactivities to attack NP and NP degradants.

3.2. Negative Polarity. In the negative polarity, the fragmentation behavior is much more straightforward because

https://doi.org/10.1021/acsomega.4c04923
ACS Omega 2024, 9, 36600−36608

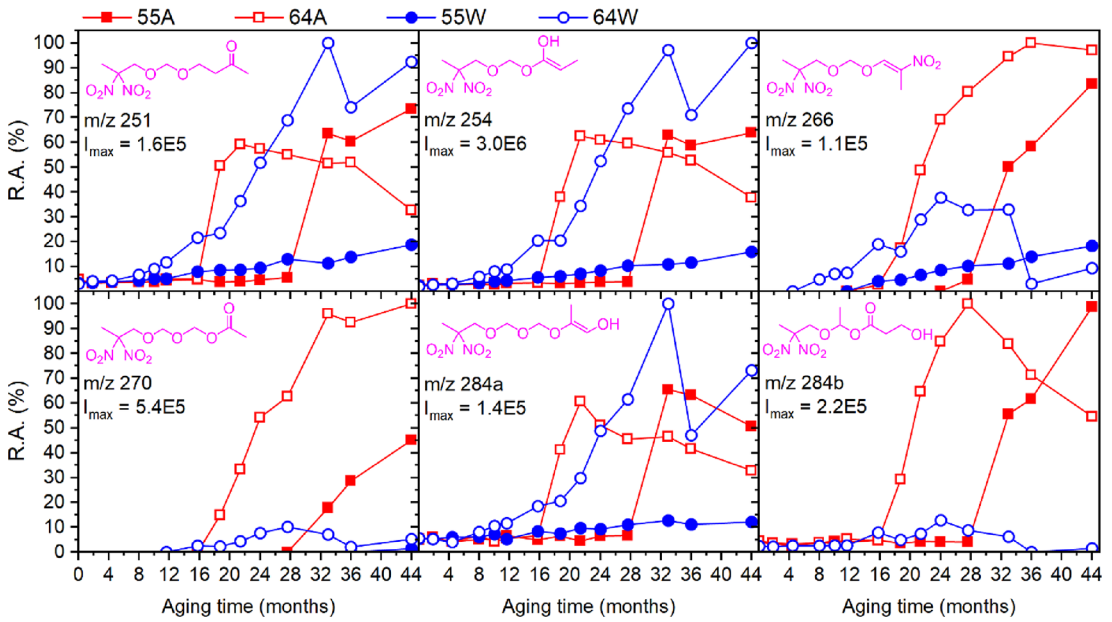

Figure 5. Time evolution of m/z 251, 254, 266, and 270 and the isomer pair at m/z 284 in the air-aged (A, red) and water-aged (W, blue) NP samples at 55 °C (solid) and 64 °C (hollow).

Scheme 2. Proposed Formation of NP Degradants from Acid-Catalyzed Hydrolysis of NP: Nucleophilic Attack of the Fragment on the Oxonium Ion

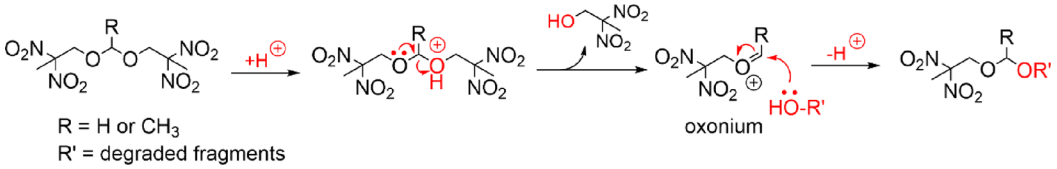

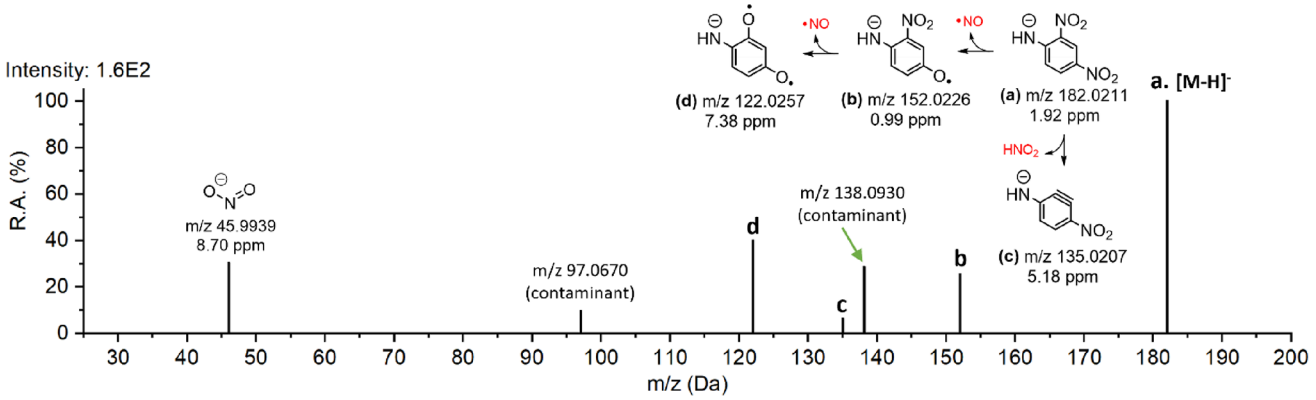

Figure 6. Representative fragment ion spectrum of m/z 182 (dinitroaniline, $[C_6H_5N_3O_4–H]^-$, T_R at 4.48 min). Homolytic loss of NO: **a** (m/z 182) → **b** (m/z 152) and → **d** (m/z 122). HONO elimination: **a** → **c** (m/z = 135). NO_2^- ion: m/z 45. m/z 138 ($C_8H_{12}NO^-$ and $C_6H_{10}N_4^-$ with 4.07 and 13.80 ppm mass errors, respectively) and m/z 97 ($C_6H_9O^-$ and $C_4H_7N_3^-$ with 11.45 and 25.28 ppm mass errors, respectively) are proposed as contaminant ions.

they are conjugated compounds containing NO_2 moieties, as shown in Figures 6 and 7. The typical loss of NO_2 or NO radicals accompanied by the elimination of CO is observed, and the ring structures tend to stay intact as a result of greater ion stability.[44] The positions of nitro groups are only tentatively assigned because a more advanced MS technique such as energy-resolved CID measurements will be required to differentiate the positions.[45] These PBNA degradants are identified as dinitroaniline (m/z 182) and dinitronaphthol (m/z 233) and only detected in the water-aged samples in the late-stage of NP aging, which were proposed as the alternative products in the hydrolysis mechanism of PBNA derivatives and not detected in our previous work.[19] The time evolutions of dinitroaniline and dinitronaphthol across various temperatures are presented in Figure 8. The formation of these two hydrolyzed products occurs almost simultaneously with higher orders of PBNA nitration, e.g., trinitro- and tetranitro-PBNAs, which is indicated by their monotonic increases of relative intensities at 38, 45, and 55 °C (<28 months). At elevated temperatures (≥55 °C), particularly at 64 °C, the association between the hydrolyzed

https://doi.org/10.1021/acsomega.4c04923
ACS Omega 2024, 9, 36600−36608

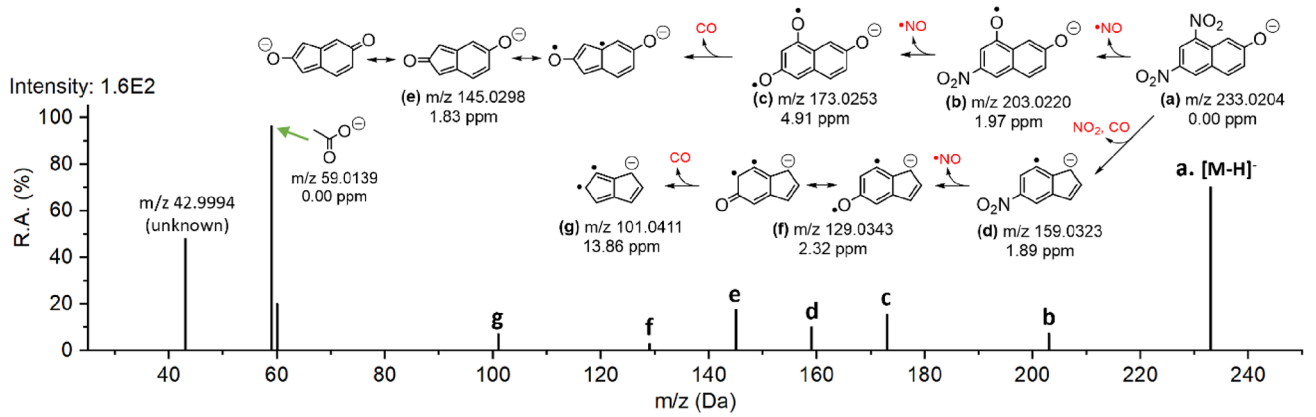

Figure 7. Representative fragment ion spectrum of m/z 233 (dinitronaphthol, $[C_{10}H_6N_2O_5-H]^-$, T_R at 3.96 min). Homolytic loss of NO: **a** (m/z 233) → **b** (m/z 203) → **c** (m/z 173) and **d** (m/z 159) → **f** (m/z 129). Loss of CO: **c** → **e** (m/z 145) and **f** → **g** (m/z 101). Concerted loss of NO_2 and CO: **a** → **d.** Acetate ion: m/z 59. m/z 43 is proposed as a background ion of unknown origin (no candidate matches within a 100 ppm mass accuracy).

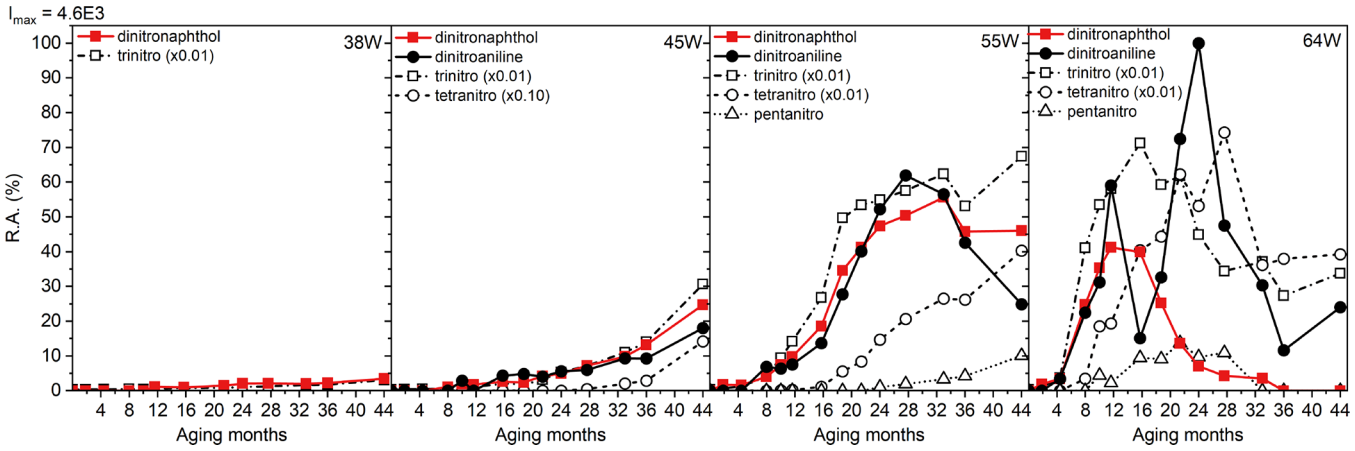

Figure 8. Time evolution of dinitronaphthol (red square), dinitroaniline (black circle), trinitro-PBNA (hollow square), tetranitro-PBNA (hollow circle), and pentanitro-PBNA (hollow triangle) in water-aged samples at 38, 45, 55, and 64 °C. The RAs of trinitro-PBNA (0.01 multiplier across all temperatures) and tetranitro-PBNA (0.10 and 0.01 multipliers for 45 and ≥55 °C, respectively) are scaled down for better qualitative comparison.

products and the nitrated PBNAs become more convoluted, possibly due to other complex reactions promoted by an acidic environment with abundant water molecules. In addition, the formation of dinitroaniline and dinitronaphthol is not confined to one unique species as there are different isomeric forms of trinitro-, tetranitro-, or pentanitro-PBNAs.

4. CONCLUSIONS

Both positive and negative ESI modes were utilized to increase the coverage of degradation species in the 44 month NP aging experiment. Through the examination of tandem MS spectrometric information, in addition to previous findings,[19−23] eight more compounds have been identified as degradants associated with the late stage of NP degradation upon depletion of PBNA and increased acid concentration: one BDNPA-related, five BDNPF-related, and two PBNA-related. The formation of nitro-organics from the degraded NP is found to be more prevalent without the presence of an aqueous layer in the aging process. The acid-catalyzed hydrolyses in both NP and PBNA follow analogous schemes proposed in our previous works. The hydrolyzed NP intermediate, oxonium ion, can either break down into DNPOH and acetic and formic acids or react with a nucleophilic degradation component. The proposed CID-based signature features and dissociation behaviors in the positive polarity, alongside the mechanism of nitro-organic production in NP degradation, could enhance the understanding of nitro-organics and assist in addressing analytical challenges in related fields, such as biomass burning and combustion emission.[1−3] Future focus will be directed to the expansion of the chemical profile and the compilation of a spectral library for NP samples aged under various conditions.

■ ASSOCIATED CONTENT

Supporting Information

The Supporting Information is available free of charge at https://pubs.acs.org/doi/10.1021/acsomega.4c04923.

Aging sample preparation; E_{cm} calculation; elucidation of fragment ion spectra of m/z 251, 254, and 284a (Figures S1−S3); and intensity profile (Tables S1 and S2) of late-stage degradants (PDF)

■ AUTHOR INFORMATION

Corresponding Authors

Kitmin Chen − *MST-7: Engineered Materials, Material Sciences and Technology Division, Los Alamos National Laboratory, Los Alamos, New Mexico 87545, United States;* orcid.org/0000-0002-1869-7147; Email: kitminc@lanl.gov

https://doi.org/10.1021/acsomega.4c04923
ACS Omega 2024, 9, 36600−36608

Dali Yang − *MST-7: Engineered Materials, Material Sciences and Technology Division, Los Alamos National Laboratory, Los Alamos, New Mexico 87545, United States;* orcid.org/0000-0003-4887-6717; Email: dyang@lanl.gov

Complete contact information is available at: https://pubs.acs.org/10.1021/acsomega.4c04923

Notes

The authors declare no competing financial interest.

■ ACKNOWLEDGMENTS

We thank Joel D. Kress for his feedback on the manuscript; Alexander S. Edgar , Justine Yang, and Camille Wong for their experimental work preceding this publication, which Alex Edgar in particular shared his valuable experience on LCMS technique and NP degradation; Kevin Morris (Consolidated Nuclear Security Pantex) for his parallel work of NP evaluation; and Katharine Orr for helping to retrieve the LC/QTOF data. Finally, we thank Dr. Phil Leonard, although no longer with us, for sharing his valuable inputs on NP hydrolysis and PBNA nitration. This work was supported by the US Department of Energy through the Los Alamos National Laboratory Aging and Lifetimes Program. The Los Alamos National Laboratory is operated by Triad National Security, LLC, for the National Nuclear Security Administration of U.S. Department of Energy (Contract 89233218CNA000001).

■ REFERENCES

(1) Rana, M. S.; Guzman, M. I. Oxidation of Catechols at the Air-Water Interface by Nitrate Radicals. *Environ. Sci. Technol.* **2022**, *56* (22), 15437−15448.

(2) Rana, M. S.; Bradley, S. T.; Guzman, M. I. Conversion of Catechol to 4-Nitrocatechol in Aqueous Microdroplets Exposed to O3 and NO2. *ACS ES&T Air* **2023**, *1* (2), 80−91.

(3) Al-Abadleh, H. A.; Motaghedi, F.; Mohammed, W.; Rana, M. S.; Malek, K. A.; Rastogi, D.; Asa-Awuku, A. A.; Guzman, M. I. Reactivity of aminophenols in forming nitrogen-containing brown carbon from iron-catalyzed reactions. *Commun. Chem.* **2022**, *5* (1), 112.

(4) Bhanot, P.; Celin, S. M.; Sreekrishnan, T. R.; Kalsi, A.; Sahai, S. K.; Sharma, P. Application of integrated treatment strategies for explosive industry wastewater—A critical review. *Journal of Water Process Engineering* **2020**, *35*, No. 101232.

(5) Guzman, M. I.; Pillar-Little, E. A.; Eugene, A. J. Interfacial Oxidative Oligomerization of Catechol. *ACS Omega* **2022**, *7* (40), 36009−36016.

(6) Rana, M. S.; Guzman, M. I. Surface Oxidation of Phenolic Aldehydes: Fragmentation, Functionalization, and Coupling Reactions. *J. Phys. Chem. A* **2022**, *126* (37), 6502−6516.

(7) Kumari, D.; Balakshe, R.; Banerjee, S.; Singh, H. Energetic plasticizers for gun & rocket propellants. *Review Journal of Chemistry* **2012**, *2* (3), 240−262.

(8) Pauler, D. K.; Henson, N. J.; Kress, J. D. A mechanism for the decomposition of dinitropropyl compounds. *Phys. Chem. Chem. Phys.* **2007**, *9* (37), 5121−6.

(9) Pesce-Rodriguez, R. A.; Miser, C. S.; McNesby, K. L.; Fifer, R. A.; Kessel, S.; Strauss, B. D. Characterization of Solid Propellant and Its Connection to Aging Phenomena. *Appl. Spectrosc.* **1992**, *46* (7), 1143−1148.

(10) Salazar, M. R.; Kress, J. D.; Lightfoot, J. M.; Russel, B. G.; Rodin, W. A.; Woods, L. Experimental Study of the Oxidative Degradation of PBX 9501 and its Components. *Propellants, Explosives, Pyrotechnics* **2008**, *33* (3), 182−202.

(11) Salazar, M. R.; Kress, J. D.; Lightfoot, J. M.; Russell, B. G.; Rodin, W. A.; Woods, L. Low-temperature oxidative degradation of PBX 9501 and its components determined via molecular weight analysis of the Poly[ester urethane] binder. *Polym. Degrad. Stab.* **2009**, *94* (12), 2231−2240.

(12) Désilets, S.; Villeneuve, S. Trace Determination of Strong Acids in NitroPlasticizers. *Analyst* **1997**, *122* (9), 995−998.

(13) Provatas, A. *Energetic Polymers and Plasticisers for Explosive Formulations − A Review of Recent Advances*; DSTO Aeronautical and Maritime Research Laboratory: Melbourne, **2000**, 51.

(14) Yang, D.; Pacheco, R.; Edwards, S.; Henderson, K.; Wu, R.; Labouriau, A.; Stark, P. Thermal stability of a eutectic mixture of bis(2,2-dinitropropyl) acetal and formal: Part A. Degradation mechanisms in air and under nitrogen atmosphere. *Polym. Degrad. Stab.* **2016**, *129*, 380−398.

(15) Wong, C. H.; Edgar, A. S.; Yang, D. Liquid Chromatography Mass Spectrometry Study of a Eutectic Mixture of bis(2,2-Dinitropropyl) Acetal/Formal. *Propellants, Explosives, Pyrotechnics* **2021**, *46* (12), 1849−1859.

(16) Yang, D.; Edgar, A. S.; Torres, J. A.; Adams, J. C.; Kress, J. D. Thermal Stability of a Eutectic Mixture of Bis(2,2-dinitropropyl) Acetal and Formal: Part C. Kinetic Compensation Effect. *Propellants, Explosives, Pyrotechnics* **2021**, *46* (1), 134−149.

(17) Yang, D.; Pacheco, R.; Edwards, S.; Torres, J.; Henderson, K.; Sykora, M.; Stark, P.; Larson, S. Thermal stability of a eutectic mixture of bis(2,2-dinitropropyl) acetal and formal: Part B. Degradation mechanisms under water and high humidity environments. *Polym. Degrad. Stab.* **2016**, *130*, 338−347.

(18) Yang, D.; Zhang, D. Z. Role of water in degradation of nitroplasticizer. *Polym. Degrad. Stab.* **2019**, *170*, No. 109020.

(19) Chen, K.; Edgar, A. S.; Jung, J.; Kress, J. D.; Wong, C. H.; Yang, D. Liquid Chromatography Quadrupole Time-of-Flight Mass Spectrometry Analysis of Eutectic Bis(2,2-dinitropropyl) Acetal/Formal Degradation Profile: Nontargeted Identification of Antioxidant Derivatives. *ACS Omega* **2022**, *7* (39), 35316−35325.

(20) Chen, K.; Edgar, A. S.; Li, Z. H.; Marina, O. C.; Yang, D. Roles of HNOx and Carboxylic Acids in the Thermal Stability of Nitroplasticizer. *ACS Omega* **2023**, *8* (16), 14730−14741.

(21) Yang, D.; Chen, K.; Edgar, A. S.; Matanovic, I.; Jung, J.; Kress, J. D. Recent progress in aging studies of a eutectic mixture of bis(2,2-dinitropropyl) acetal and formal nitroplasticizer. *Polym. Degrad. Stab.* **2023**, *218*, No. 110565.

(22) Chen, K.; Kress, J. D.; Yang, D. New insight: Nitrosation of n-phenyl-β-naphthylamine in the early stage of nitroplasticizer aging. *Polym. Degrad. Stab.* **2023**, *217*, No. 110541.

(23) Edgar, A. S.; Wong, C. H.; Chen, K.; Langlois, D. A.; Yang, D. Identification of 2,2-dinitropropanol, a Hydrolyzed Product of Aged Eutectic Bis(2,2-dinitropropyl) Acetal − Bis(2,2-dinitropropyl) Formal Mixture. *Propellants, Explos., Pyrotech.* **2022**, *47* (10), No. e202100345.

(24) Freye, C. E.; Snyder, C. J. Investigation into the Decomposition Pathways of an Acetal-Based Plasticizer. *ACS Omega* **2022**, *7* (34), 30275−30280.

(25) Chen, K.; Yang, D. *Fast Semi-automated Postprocessing Workflow of Untargeted LC-QTOF-MS Data for Aging Study*. LA-UR-23−20482. Los Alamos National Laboratory: Los Alamos, NM, 87545, 2023.

(26) Yinon, J. Analysis and Detection of Explosives by Mass Spectrometry. In *Aspects of Explosives Detection*; Elsevier: **2009**.

(27) Yinon, J.; McClellan, J. E.; Yost, R. A. Electrospray ionization tandem mass spectrometry collision-induced dissociation study of explosives in an ion trap mass spectrometer. *Rapid Commun. Mass Spectrom.* **1997**, *11* (18), 1961−1970.

(28) Oberacher, H.; Sasse, M.; Guitton, Y.; Antignac, J. P.; Debrauwer, L.; Jamin, E.; Schulze, T.; Krauss, M.; Covaci, A.; Caballero-Casero, N.; Rousseau, K.; Damont, A.; Fenaille, F.; Lamoree, M.; Schymanski, E. L. A European proposal for quality control and quality assurance of tandem mass spectral libraries. *Environ. Sci. Eur.* **2020**, *32*, 43.

(29) Khreis, J. M.; Pandeti, S.; Feketeová, L.; Denifl, S. High-energy collision-induced dissociation of radiosensitizer anions: Nimorazole and metronidazole. *Int. J. Mass Spectrom.* **2018**, *431*, 1−7.

(30) Paine, M. R. L.; Kirk, B. B.; Ellis-Steinborner, S.; Blanksby, S. J. Fragmentation pathways of 2,3-dimethyl-2,3-dinitrobutane cations in

the gas phase. *Rapid Commun. Mass Spectrom.* **2009**, *23* (18), 2867−2877.
(31) Chandran, J.; Aravind, U. K.; Rajalakshmi, C.; Thomas, V. I.; Nguyen, P. T.; Aravindakumar, C. T. Solvent dependent ESI-collisionally induced dissociation of protonated nitenpyram. *Int. J. Mass Spectrom.* **2019**, *445*, No. 116207.
(32) Levsen, K.; Schiebel, H. M.; Terlouw, J. K.; Jobst, K. J.; Elend, M.; Preiss, A.; Thiele, H.; Ingendoh, A. Even-electron ions: a systematic study of the neutral species lost in the dissociation of quasi-molecular ions. *J. Mass Spectrom.* **2007**, *42* (8), 1024−44.
(33) Dewar, M. J. S.; Ritchie, J. P.; Alster, J. Ground states of molecules. 65. Thermolysis of molecules containing NO2 groups. *Journal of Organic Chemistry* **1985**, *50* (7), 1031−1036.
(34) Zhang, C.; Wang, X.; Zhou, M. Isomers and isomerization reactions of four nitro derivatives of methane. *J. Comput. Chem.* **2011**, *32* (8), 1760−1768.
(35) Carrasco, E.; Tanarro, I.; Herrero, V. J.; Cernicharo, J. Proton transfer chains in cold plasmas of H2with small amounts of N2. The prevalence of NH4+. *Phys. Chem. Chem. Phys.* **2013**, *15* (5), 1699−1706.
(36) Heninger, M.; Lauvergnat, D.; Lemaire, J.; Boissel, P.; Mauclaire, G.; Marx, R. Radiative lifetime of vibrationally excited N2H+ and N2D + molecular ions. *Int. J. Mass Spectrom.* **2003**, *223−224*, 669−678.
(37) Qian, K.; Shukla, A.; Futrell, J. Observation of isolated electronic states in the collision-induced dissociation of nitromethane ions. *Rapid Commun. Mass Spectrom.* **1990**, *4* (6), 222−224.
(38) Demarque, D. P.; Crotti, A. E.; Vessecchi, R.; Lopes, J. L.; Lopes, N. P. Fragmentation reactions using electrospray ionization mass spectrometry: an important tool for the structural elucidation and characterization of synthetic and natural products. *Nat. Prod. Rep.* **2016**, *33* (3), 432−55.
(39) Clayden, J.; Greeves, N.; Warren, S. Nucleophilic Substitution at C = O with Loss of Carbonyl Oxygen. In *Organic Chemistry*; 2nd ed.; Oxford University Press: New York, 2012; pp 223−228.
(40) Leonard, P. W. *Mechanism of acetal (or formal) hydrolysis (Personal Communication)*; Los Alamos National Laboratory: Los Alamos, NM, United States, 2016.
(41) Kress, J. D. *Nitroplasticizer Resistance to Hydrolysis (Personal Communication)*; Los Alamos National Laboratory: Los Alamos, NM, United States, 2006.
(42) Rindone, R.; Geiss, D. A. Jr.; Miyoshi, H. *IM/EM Technology Implementation in the 21st Century: BDNPA/BDNPF shows long-time aging stability*; November 27 − 30, 2000.
(43) Morris, K. D.; Cook, J.; Harrison, C.; Rodriguez, X. *Evaluation of Nitroplasticizer Reserves, Level 2 Milestone ID 7134. PXRPT 20−10. CNS, LLC.*; Pantex Plant: Amarillo, TX, USA. September 1, 2020.
(44) Schmidt, A. C.; Herzschuh, R.; Matysik, F. M.; Engewald, W. Investigation of the ionisation and fragmentation behaviour of different nitroaromatic compounds occurring as polar metabolites of explosives using electrospray ionisation tandem mass spectrometry. *Rapid Commun. Mass Spectrom.* **2006**, *20* (15), 2293−302.
(45) Wenthold, P. G.; Paulino, J. A.; Squires, R. R. The absolute heats of formation of o-, m-, and p-benzyne. *J. Am. Chem. Soc.* **1991**, *113* (19), 7414−7415.

https://doi.org/10.1021/acsomega.4c04923
ACS Omega 2024, 9, 36600−36608